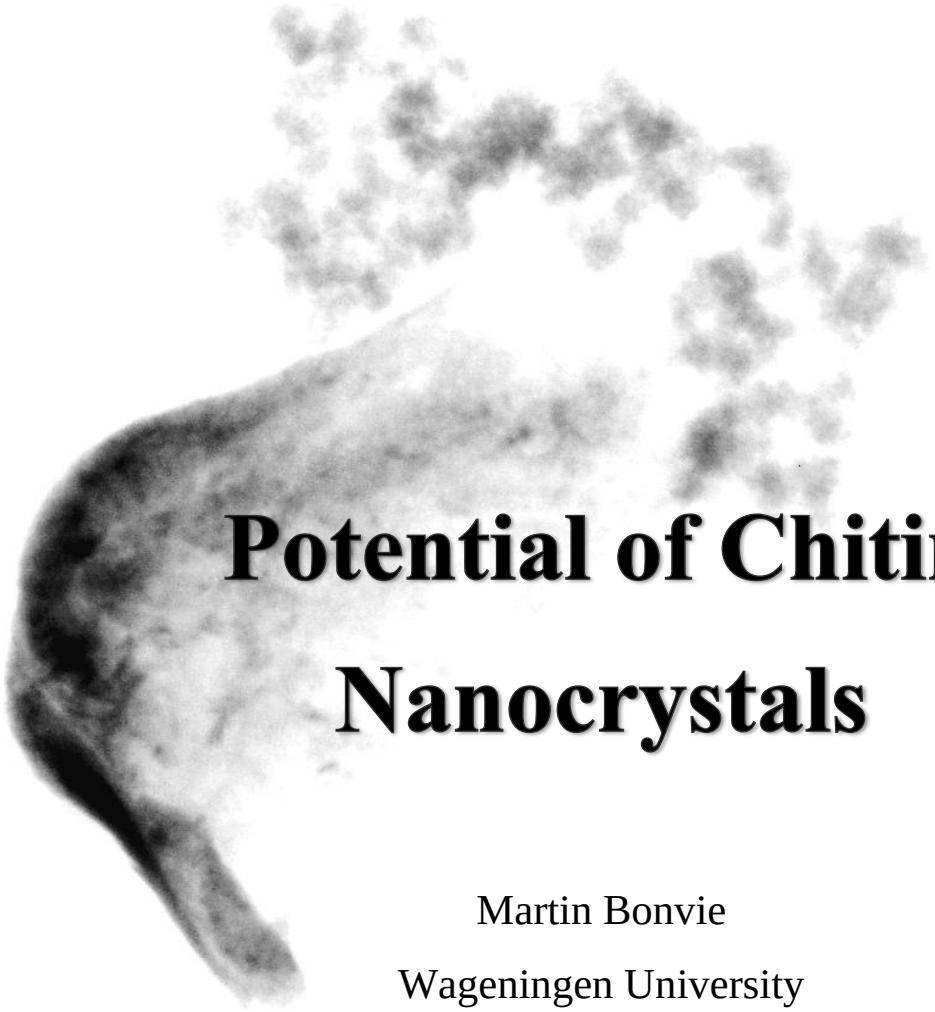

Potential of Chitin Nanocrystals

Martin Bonvie

Wageningen University

Biobased Chemistry & Technology

30th June, 2017

Project	:	MSc Thesis
Number	:	BCT-80436
Study load	:	36 ects
Date	:	1-11-2016
Student	:	Martin Bonvie
Registration number	:	860928095040
Study programme	:	MFT (Food Technology) – Sustainable Food Process Engineering
Report number	:	067BCT
Supervisor(s)	:	Costas Nikiforidis
Examiners(s)	:	Costas Nikiforidis, Elinor Scott, Tomas van Haasterecht
Group	:	Biobased Chemistry and Technology
Address	:	Bornse Weilanden 9 6708 WG Wageningen The Netherlands Tel: +31 (317) 48 21 24 Fax: +31 (317) 48 49 57

ABSTRACT

Chitin is a naturally occurring polysaccharide that can be found in shrimp shells, a waste product from food industry. Due to its abundance and interesting properties, chitin is a hot topic within both academia and industry, with research in many fields. The aim of this thesis was to explore the use of chitin as a catalyst support material. We compared the shrimp shells (SHSH) to its counterpart hydrolysed chitin nanocrystals (CHNC) as a support material for a copper catalyst. In this work, the importance of the catalyst support preparation has been investigated and the effect of drying on the properties of the copper catalyst. Drying at 60 °C resulted in homogeneous dried impregnated samples. Moreover, various reduction conditions were also studied to obtain evenly dispersed metallic copper for catalysis.

Different properties of the catalyst and its support were measured, including support material pore size and copper particle size, thermal stability and crystallinity. Thermal gravimetric analysis (TGA) showed that the degradation of SHSH began at a higher temperature than the degradation of CHNC. Transmission electron microscopy (TEM) was applied to analyse the morphology of CHNC and also the copper particle size distribution, which when embedded on a CHNC support, ranged from 15 to 25 nm. X-ray diffraction (XRD) was used to show the formation of copper oxides and metallic copper by various calcination/reduction conditions. Moreover, physisorption revealed that the surface area of the CHNC support was greater than SHSH, a beneficial property for a catalyst carrier. Considering all analysis performed, CHNC had preferable catalyst carrier properties in comparison to SHSH, however, further work is necessary to compare and evaluate copper catalysis on a CHNC support in contrast to another support system.

TABLE OF CONTENTS

Abbreviations

AFM	Atomic force microscopy
CHNC	Chitin nanocrystals
FTIR	Fourier transform infrared
HPLC	High performance liquid chromatography
IWI	Incipient wetness impregnation2
SEM	Scanning electron microscopy
SHSH	Shrimp shells
TEM	Transmission electron microscopy
TGA	Thermogravimetric analysis
XRD	X-ray diffraction

1 INTRODUCTION

Chitin is the second most abundant polysaccharide found in nature, next to cellulose, acting as a structural building block. Chitin can be found in a number of natural sources: algae, cell walls of funghi, exoskeletons of crustaceans, insects, invertebrates, marine diatoms, molluscs and yeasts (Synowiecki & Al-Khateeb, 2003). Chitin is a polymer consisting of repeating units of N-acetylglucosamine and the chemical structure is shown in Figure 1. It can be found in three different polymorphic forms: α, β, and γ. The form found is dependent upon the source and differs in the arrangement of the individual chitin chains and the resulting side chain interactions. In the α-chitin form, the chains are organised in an anti-parallel fashion, whereas in the β-form, the chains align in parallel (Jang *et al.*, 2004). Intra- and inter-chain hydrogen bonding between the N-H⋯O=C groups leads to a rigid, highly ordered crystalline structure (Jang *et al.*, 2004; Sikorski *et al.*, 2009). γ-chitin is a mixture of the two arrangements. Chitosan is a derivative of chitin, which differs in the amount of acetyl groups (CH_3CO) in the side chain; above 50 % acetylation is termed chitin, and values below are termed chitosan (Khor *et al.*, 2003).

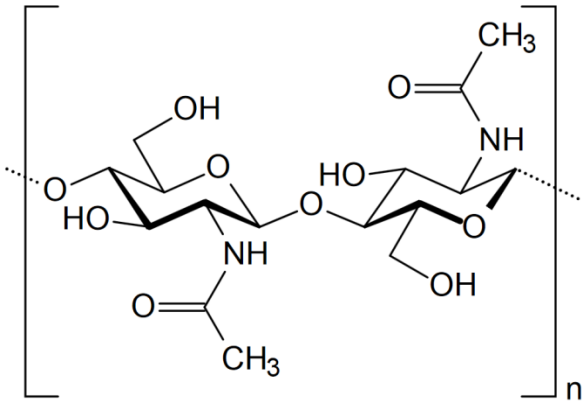

Figure 1. Chemical structure of the chitin molecule, showing two of the N-acetylglucosamine subunits that repeat to form the polysaccharide.

The largest source of chitin currently comes in the α-form as a waste stream from the food industry during preparation of shellfish. The typical composition of shellfish waste is 20-30 wt% chitin, 30-40 wt% proteins, 30-50 wt% calcium carbonate, and lipids and astaxanthin (<1 wt%) (Zeng *et al.*, 2011). The annual quantity of shellfish harvested is estimated to be 29.900.000 tonnes per year, ranging in chitin content from 2-12 wt% (wet basis) of the crustaceans total body mass (Synowiecki & Al-Khateeb, 2003). This corresponds to a minimum annual chitin production of approximately 6.000.000 tonnes, based on the lowest chitin content. Instead of sending the shrimp shells to landfill or discarding in the sea, it is potentially economically and environmentally desirable to valorise the shrimp shell waste stream (Yan & Chen, 2015).

This polysaccharide has a number of interesting properties that has led to increased interest within academia and industry, especially in the fields of biomedicine and food. According to Yu *et al.* (2014), chitin has excellent mechanical properties due to its light weight and high strength,

as well as good biocompatibility. Some examples of the applications of chitin within the literature include: emulsion stabilisation (Perrin *et al*., 2014), wound healing and drug delivery (Khor & Lim, 2003), fruit juice clarification and gel formation (Rinaudo, 2006). Several studies showed the use of chitin as a biosorption material for the removal of heavy metals during waste water treatment. Pinto *et al.* (2011) investigated two commercially available chitin products for heavy metal removal during waste water treatment from mining. Under alkali and neutral conditions, it was possible to completely remove iron, lead and zinc, and partially remove cadmium, cobalt, copper and manganese at a chitin load of 2 g/L (Chitorem SC-20) (Pinto *et al.*, 2011). Currently, there are many uses for chitin being explored within the literature, yet none are carried out, to the author's knowledge, on a commercial scale.

Another new promising area under investigation involves the use of materials on a nanoscale derived from natural sources, including chitin. Chitin particles on the nanoscale size range are referred to as whiskers, nanocrystals, nanofibers or nanorods. Within this thesis, chitin derivatives of a nano-size will be referred to as chitin nanocrystals (CHNC). Nanocrystals are defined by having a length or width of less than 100 nm in at least one dimension. Table 1 shows the sizes of CHNC found within the literature and also the methods utilised to measure it.

Table 1. Nanocrystal size comparison from various literature sources, including the microscopy technique used for measurement.

Length (nm)	Width (nm)	Method	Source
100-600	4-40	TEM	Gopalan Nair & Dufresne, 2003
100-700	5-30	TEM	Lin *et al.*, 2012
240	18	TEM	Tzoumaki *et al.*, 2010
200-500	10-15	TEM	Goodrich & Winter, 2007

The use of CHNC is becoming popular because of their low cost, rigidity, high aspect ratio and highly crystalline structure (Lin *et al.*, 2012). Isolated Chitin consists of a high crystalline structure compared its unhydrolysed counterpart (Zhang *et al.*, 2015). CHNC also have the additional features of a larger surface area and Young's modulus compared to crude chitin (Perrin *et al.*, 2014), thermal and chemical stability (Wang *et al.*, 2015).

To obtain CHNC, different temperatures, types of acid, acid concentration and duration have been employed in the literature, varying these conditions adjusts the degree of hydrolysis (Lin *et al.*, 2012). The principle steps to prepare CHNC include: an alkali treatment to remove contaminating proteins, bleaching to breakdown contaminating light emitting chromophore molecules, hydrolysis with an acid at an elevated temperature to reduce the chitin chain length, reducing to a nanoscale size, as well as demineralising using washing and centrifugation, and finally sonication to break up the chitin aggregates (Tzoumaki *et al.*, 2010).

CHNC have been studied for a number of different applications. Gels from natural sources have been studied due to their many applications in the food, pharmaceutical, cosmetic and paint industries (Tzoumaki *et al.*, 2010). One area of interest which has not been widely studied is the use of CHNC as a catalyst support material. For an optimum catalyst support the following criteria are necessary: large surface area, cheap, unreactive in reaction medium, thermal stability (reaction and preparation dependent), widely available, recoverable (catalyst remains on the support) and non-toxic. Little research is available on the use of chitin or CHNC as catalyst carriers in contrast to cellulose, the most abundant polysaccharide in nature. Using chitin supported ruthenium, Matsuoka *et al*. (2015) found high yields during the hydration of various nitriles to amides under aqueous conditions. As well as achieving high yields, the catalyst preparation was relatively easy and tested on a variety of nitriles with aromatic, heteroaromatic and aliphatic substituents. Wang *et al.* (2015) produced chitin microspheres by employing a sol gel method. The microspheres were loaded with the catalyst α-amylase. After using the catalyst for 10 repeated cycles, an activity of 95 % of the enzyme was still achieved.

In this thesis it is hypothesised that CHNC have superior properties as a catalyst support in contrast to crude chitin in terms of porosity and available surface area. No previous research has been found on the use of CHNC in the field of catalyst supports. The aim of this study was to examine the effects of support preparation and calcination/reduction. Analysis to gauge the success of the catalyst support includes thermal degradation analysis, physisorption, microstructural investigations and XRD to understand the most viable route to prepare chitin as a catalyst support material. Catalysis using metallic copper (Cu^0) can be employed to produce sorbitol from glucose and fructose (Liu et al., 2014b). The goal was to obtain metallic copper on the chitin support materials with the least copper oxides.

2 MATERIALS & METHODS

2.1 MATERIALS

Coarse flake shrimp shells were obtained from Sigma-Aldrich (St. Louis, MO). Distilled water was used in all experiments. Sigma-Aldrich was the supplier of hydrochloric acid (HCl, concentrated 37 % v/v), sodium acetate ($C_2H_3NaO_2$), glacial acetic acid, potassium hydroxide (KOH), sodium chlorite ($NaClO_2$), dialysis tubing cellulose membrane (cut-off: 14,000 Da), copper nitrate trihydrate ($Cu(NO_3)_2$) and chitin from shrimp shells (Sigma-Aldrich: C9752).

2.2 ISOLATION OF CHITIN NANOCRYSTALS (CHNC)

The procedure described by Tzoumaki *et al.* (2009) was altered in terms of quantity of shrimp shells used, centrifugation time and rotation speed. The nanocrystal dispersion did not settle after numerous of centrifugation attempts, therefore higher G forces were used and longer centrifugation times. In the procedure it was unclear in which step glacial acetic acid was used. Thereby the assumption has been made that the acetic acid is used to alter the pH of the sodium acetate buffer solution.

Raw shrimp shells were purified based on a protocol described by Tzoumaki *et al.* (2009) and Nair & Dufresne (2003) to obtain chitin nanocrystals (CHNC). Approximately 60 g of shrimp shells were suspended in 1400 mL of 5 % w/w KOH solution and boiled for 6 h under stirring to remove contaminating proteins. This dispersion was kept at room temperature overnight under continuous stirring. The dispersion was filtered and washed several times with distilled water with the use of a Büchner funnel. The material remaining after the above procedure, was bleached in 700 mL of a $NaClO_2$ solution (17 g of $NaClO_2$ in 1 L of 0.3 M sodium acetate buffer, the pH was adjusted to 4.0 with the use of glacial acetic acid), at 80 °C for 6 h. The bleaching solution was changed every 2 h, followed by rinsing the sample with distilled water. Subsequently, the resulting material was kept in approximately 700 mL of 5 % w/w KOH solution for 48 h to remove any residual proteins. The resulting dispersion was centrifuged at 2500 × *g* for 15 min. The chitin nanocrystal dispersion was prepared by hydrolysing the purified chitin sample with 3 N HCl at a boiling temperature for 90 min under continues stirring. The ratio of 3 N HCl to chitin solids was 30 mL /g chitin. After acid hydrolysis, the dispersion was diluted with distilled water and followed by centrifugation at 2500 × *g* for 15 min. This centrifugation process was repeated three times. Afterward, the dispersion was transferred to a dialysis bag and dialyzed under running tap water for 2 h and left overnight into distilled water. Appropriate volumes of 1 N HCl solution were used to adjust the final pH of the dispersion to 3. To break the possible CHNC aggregates, the dispersion was finally subjected to an ultrasonic treatment for 45 min. To avoid overheating of the sample, intervals of 5 min were given. The nanocrystals were subsequently stored at 4 °C.

2.3 FREEZE DRYING

The procedure by Tzoumaki *et al*. (2009) resulted in the production of an aqueous dispersion. For further analysis and impregnation, the nanocrystals had to be dried. Freeze drying was chosen as the most sensible route to produce dried CHNC. Prior to freeze drying the samples were frozen at -20 °C. Wu & Meredith (2014) investigated different freezing temperatures of chitin nanofibers prior to freeze drying (-20,-80 and -196 °C); the highest temperature for freezing resulted in the smallest pore size in a range of 0.33 – 3.2 µm.

The chitin dispersions were stored at -20 °C for 24 h before freeze drying. The frozen chitin was further cooled down to −80 °C and then dried in a freeze-dryer (Christ alpha 2-4 LDplus) at 0.011 mbar for 48 h and for the final drying step at 0.001 mbar for 24 h.

2.4 FOURIER TRANSFORM INFRARED SPECTROSCOPY (FTIR)

To confirm the correct functional groups are present within the samples, Fourier Transform Infrared Spectroscopy (FTIR) was used to compare to literature, FTIR spectra of the samples were obtained on a Varian Scimitar 1000 FT-IR spectrometer equipped with a DTSG-detector and a PIKE MIRacle ATR. The sample was placed on a diamond w/ZnSe lens single reflection plate. The measurement resolution was set at 4 cm^{-1}, and the spectra were collected in the ATR (Attenuated Total Reflection) mode in the range 4000-650 cm^{-1} with 64 co-added scans. The obtained data were transferred into excel for further analysis.

2.5 CATALYST IMPREGNATION, INCIPIENT WETNESS IMPREGNATION (IWI)

Dry CHNC and SHSH were impregnated with an aqueous solution of copper nitrate trihydrate. To achieve a sufficient wetness, liquid was added to the catalyst support dropwise until complete saturation on a visual basis. A liquid/support ratio of 3.6 mL/g was determined for both CHNC and SHSH. To obtain a 5 wt% copper solution to add to the support, it was calculated that 19 g of copper nitrate trihydrate was required, based on molar masses. After impregnation, the samples were dried for 3 h at 60 °C, and will be referred to as 5Cu-CHNC and 5Cu-SHSH for impregnated CHNCand impregnated chitin from shrimp shells, respectively.

2.6 CALCINATION/REDUCTION

Calcination/reduction of the catalyst impregnated support was done in a tubular furnace. A quartz weighing boat was used to carry the catalyst/support which weighed about 1 g ±0.3. The sample was heated with a heating rate of 5 °C/min to 250 °C and left for 2 h. A gas hourly space velocity (GHSV) of 26 % N_2 and 30 % H_2 was used. Afterwards the H_2 flow was turned off and flushed for 30 min with N_2 to clear out the volatile and harmful H_2 gas.

A 5 wt% Cu sample was prepared by impregnation of the hydrolysed chitin support to incipient wetness (see section 2.5). Two different routes were taken, (i) direct reduction and a (ii) two-step

reduction. The first route (i) involved transferring the impregnated sample to a tubular oven, where the sample was heated to 250 °C (5 °C min^{-1}) in a the gas hourly space velocity (GHSV) during thermal treatment, N_2/ H_2, air, or N_2 was used and subsequently left in the same gas flow for 2 h. Alternatively (ii), the impregnate was dried at 200 °C in a static air oven for 2 h and the sample is subsequently reduced in a tubular oven with a flow of N_2/H_2, air, or N_2. Equations 1-4 show the intermediate steps (impregnation, drying, calcination and reduction) necessary to obtain metallic copper.

Impregnation $$Cu(NO_3)_2 \cdot 3H_2O\ (s) \longrightarrow Cu^{2+}(aq) + 2NO_3{}^{-}(aq) + xH_2O\ (aq) \quad (1)$$

Drying $$Cu^{2+}(aq) + 2NO_3{}^{-}(aq) + xH_2O\ (aq) \longrightarrow Cu(NO_3)_2\ (s) + xH_2O \quad (2)$$

Calcination $$Cu(NO_3)_2(s) \longrightarrow CuO(s) + NO_x\ (g) \quad (3)$$

Reduction $$CuO\ (s) \xrightarrow{Hydrogen} Cu\ (s) + xH2O \quad (4)$$

The calcination/reduction temperatures was held at the given temperature °C for 2 h.

Various conditions of drying and calcination/reduction were tested to study the preparation effects on the resulting impregnated samples. These conditions can be found in Table 2. In this thesis, chitin nanocrystal samples (CHNC) are denoted as CHNC-X, where X stands for the gas or gas combination used during reduction and/or calcination. This principle accounts the same for shrimp shells (SHSH) these are denoted as SHSH-x. CHNC reduced in H_2 (g) are denoted as CHNC-H2 or SHSH-H2, respectively. Impregnated samples denoted with "5*Cu"*, corresponds to 5 % copper impregnation to the support material. Thus samples denoted as 5Cu-CHNC-H2 refers to 5 % copper impregnated onto a CHNC support and reduced with hydrogen gas.

Table 2. Sample preparation, drying temperature/time and metal particle size in the impregnated Cu/CHNC samples.

	Drying		**Calcination/reduction**		
Sample	Temp (°C)	Duration (h)	Temp (°C)	Gas	GHSV (mL/min)
5Cu-CHNC	120	3	250	N_2/H_2	63/30
5Cu-CHNC	60	4	200	N_2/H_2	63/30
5Cu-CHNC	60	4	150	N_2/H_2	63/30
5Cu-SHSH	120	3	250	N_2	63
5Cu-SHSH	60	3	200	H_2	30
5Cu-SHSH	120	3	200	N_2/H_2	63/30
5Cu-SHSH	60	3	200	Air	-

2.7 THERMAL DEGRADATION (TGA)

To determine the degradation temperature profiles a TGA/DSC1 STARe system Mettler Toledo was used. The initial mass of each sample was 10 ± 0.5 mg and placed into a 70 µL aluminium crucible without lid, then loaded into the TGA and heated from 30 °C to 900 °C. The degradation temperature of the samples were studied at a heating rate of 20 °C/min in a nitrogen atmosphere with a purge rate of 50 mL/min. Data was acquired by means of *STARe* software and analysed using Microsoft Excel.

2.8 X-RAY DIFFRACTION (XRD)

To determine the crystallinity of the nanomaterials and catalyst, powder X-ray diffraction patterns were obtained by means of X-ray diffraction (XRD). With the use of the following operating conditions: 40 kV, 40mA, the relative intensity was recorded at a scattering range (2θ) of 10° to 90°. The measuring time was 1s/step. Crystal lattices and their specific peaks can be compared with the measured samples.

2.9 TRANSMISSION ELECTRON MICROSCOPY (TEM)

Transmission electron microscopy imaging was performed on a JEOL JEM-2000FX transmission electron microscope operated at an acceleration voltage of 80 kV. One drop of the CHNC in methanol suspension (0.025 w/w %) was deposited on a carbon-coated copper grid and allowed to air dry. Optical micrographs of the CHNC dispersions were captured by an Olympus BX 51 polarizing optical microscope fitted with a digital camera (Olympus, DP 50). The specimens were prepared by placing a thin layer of sample between a microscope slide and a coverslip.

2.10 SCANNING ELECTRON MICROSCOPY (SEM)

The surface morphology of dry samples suspended in HPLC grade methanol was determined using a scanning electron microscope (SEM). The samples were mounted on an aluminium mount and sputtered with tungsten. The samples were scanned at an accelerating voltage of 10 kV, with a working distance of ±40 mm, as appropriate. EDX measurements were taken throughout various scans to determine the localisation of various elements within the samples.

2.11 PHYSISORPTION

Both adsorption and desorption isotherms were measured with the Micromeritics TriStar II plus. The samples were dried overnight at high vacuum at 120 °C prior to measurement with nitrogen. The specific surface areas were calculated according to the Brunauer-Emmett-Teller (BET) method.

3 RESULTS & DISCUSSION

3.1 CHITIN NANOCRYSTALS AND SHRIMP SHELL PREPARATION

The procedure to obtain CHNC is an adaptation from the procedure presented by Tzoumaki *et al.* (2009). The resultant CHNC that were produced after acid hydrolysis, purification and freeze drying the hydrolysed were fluffy and white, the structure can be seen in Figure 2.

Figure 2. Photograph of chitin nanocrystals (CHNC) after freeze drying.

3.1.1 FTIR

To ensure that a pure CHNC sample had been prepared, FTIR was used to identify the functional groups that were present. Figure 3 shows the spectra recorded for SHSH, CHNC and a reference SHSH of the samples show a similar FTIR spectra, all of the peaks present in the reference sample are present in the SHSH and CHNC sample. Previously in the literature (Goodrich & Winter, 2007), the FTIR spectra of crude chitin and CHNC have been presented. The assignment of the peaks at 1656, 1621 & 1556 cm^{-1} correspond to two amide regions within the chitin chain

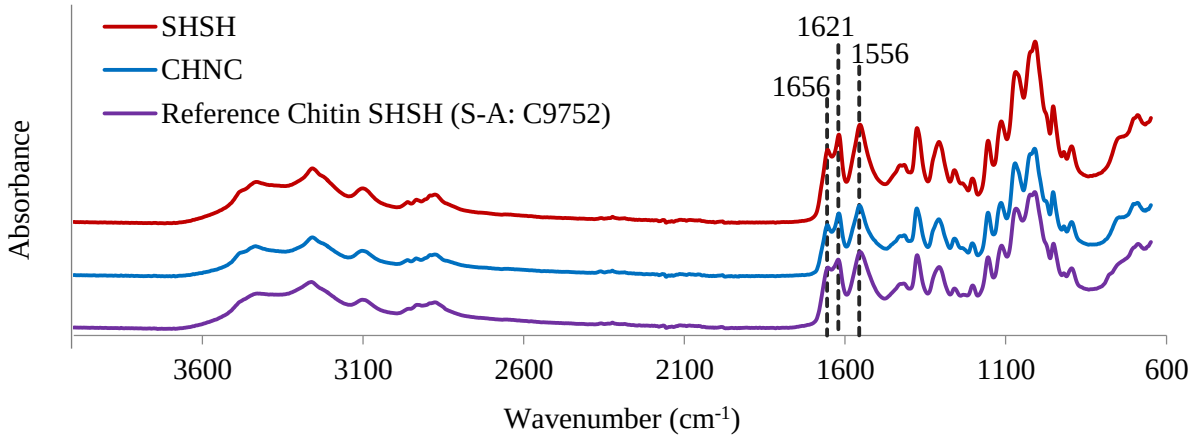

Figure 3. FTIR spectra of various chitin based samples. Shrimp shells (SHSH), chitin nanocrystals (CHNC). Amide peaks are assigned using a literature source (Goodrich & Winter, 2007).

Structure (Goodrich & Winter, 2007). These spectra indicate that the crude chitin was already pure without contamination from protein or any other substance. An assumption is made that the deprotonation step with KOH in the procedure of Tzoumaki *et al*. (2010) can be discarded in future work.

3.1.2 TGA

Thermal gravimetric analysis (TGA) gives us information about the degradation of samples during thermal treatment. This is useful information because if the calcination/reduction after impregnation is carried out at temperatures above the degradation temperature of the catalyst carrier, then the support is not suitable. This is also useful information for if the reaction to be catalysed occurs at elevated temperatures.

Figure 4 shows the TGA profiles of pyrolysis for CHNC and crude chitin SHSH at a heating rate of 20 °C/min. The onset of water evaporation was coupled with weight-loss centred at about 100 °C (Wanjun *et al.*, 2005). From Figure 4, the water content of SHSH and CHNC can be measured as 5 % and 3 %, respectively.

For SHSH, the onset of chitin degradation occurred at 265 °C, compared to CHNC which occurred at 215 °C. It was found that 61 % of the CHNC was degraded during the second weight loss episode in the TGA curve. The weight loss for SHSH during heating up to 370 °C was measured at 66 %. The thermal stability of chitin is lower than that of crude chitin sample (SHSH), as degradation occurred at a lower temperature. At these temperatures, depolymerisation of the chitin occurs, which resulted in the production of volatile components and char (Wanjun *et al.*, 2005). Köll *et al.* (1991) confirmed that the deacetylation of chitin, which increased with increasing temperature, was not the largest contributing factor to weight loss. The degree of acetylation was measured using HPLC. This means that inter-chain hydrogen bonding is still present between the chitin chains after thermal treatment.

The maximum decomposition temperature of α-chitin was found in the literature to have a value of 419.4 °C at a heating rate of 20 °C/min (Jang *et al.*, 2004). Changes to the heating rate during TGA leads to variation in the maximum decomposition temperature (T_m). The maximum decomposition temperature of CHNC found within this thesis is comparable to the literature source measured at the same heating rate (Jang *et al.*, 2004).

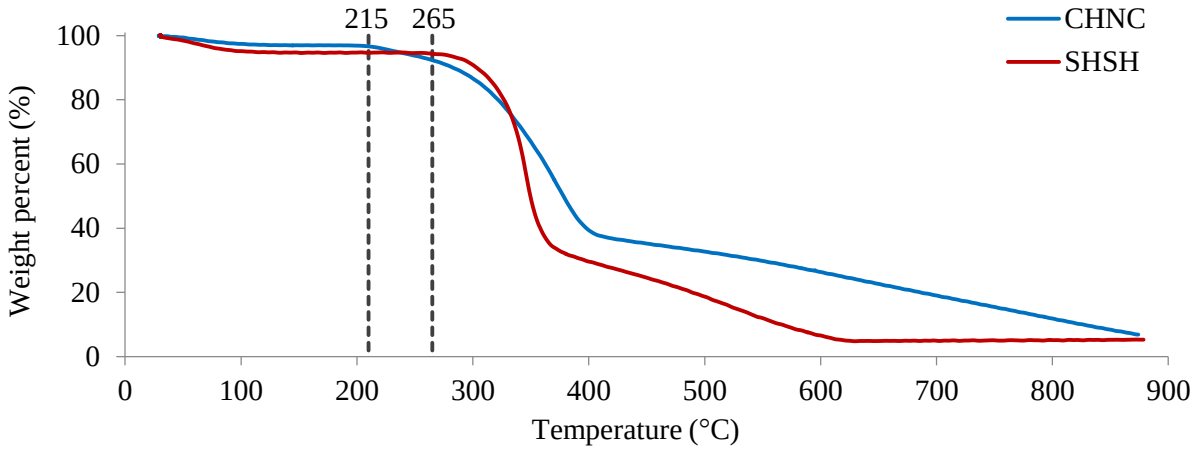

Figure 4. TGA curves to show the effect of increasing temperature at a rate of 20 °C/min on the degradation of chitin nanocrystals (CHNC) and shrimp shells (SHSH).

3.1.3 XRD

The intensity and position of the peaks in an XRD pattern provides information on the crystal structure of the examined sample. XRD patterns were recorded to compare the effects of CHNC preparation versus the crude SHSH prior to hydrolysis. The comparison can be seen in Figure 5, including the annotation of the observed 2Theta values. The XRD patterns for CHNC and the crude SHSH contained peaks at similar 2Theta values. Crystallinity of CHNC has also been studied previously in the literature (Goodrich & Winter, 2007), including the assignment of 2Theta values to crude shrimp shells and CHNC to peaks measured in the range of 7-30°. Similar 2Theta values were also found for CHNC prepared by Liu *et al.* (2014a) for use in waste water treatment. These 2Theta values are similar to those found within this study (Table 3). The peaks within the XRD pattern correspond to the Miller indices (hkl), which correspond to different planes within the molecule under investigation. Different planes intersect atoms differently, hence why a number of peaks are seen per crystal structure.

The intensity of the peak at the 2Theta value of 19.36° was greater for CHNC than for SHSH, indicating a difference in the crystallinity between the two samples. The preparation of CHNC resulted in the formation of a more crystalline material than SHSH, confirmed by XRD. This was also found by Goodrich & Winter (2007), where acid hydrolysis resulted in an increase of crystallinity of chitin by 8 %. This value was measured as the ratio of the sum of areas under the crystalline diffraction peaks of chitin to the total area under the curve.

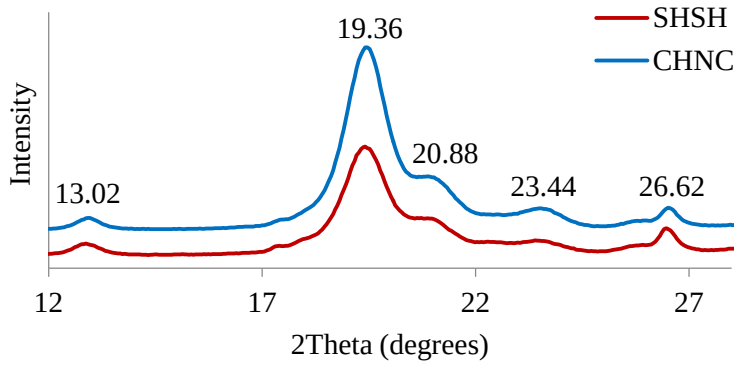

Figure 5. A comparison of XRD patterns of crude shrimp shells (SHSH) and chitin nanocrystals (CHNC).

Table 3. Observed and literature (Goodrich & Winter, 2007) reported 2Theta values

2Theta$_{literature}$	**2Theta$_{observed}$**
12.82	13.02
19.40	19.36
20.88	20.88
22.47	23.44
26.65	26.62

3.1.4 Transmission electron microscopy (TEM)

To characterise the CHNC, TEM was carried out to determine the size and organisation of the nanocrystals. Table 1 shows the size ranges of CHNC found within the literature. Figure 6A shows a transmission electron micrograph (TEM) of a dilute suspension 0.025 wt% of CHNC. TEM confirms the presence of evenly dispersed CHNC in the sample. Within this study, it was not possible to measure the length or width of the crystals due to oversaturation. Tzoumaki *et al*. (2010) made a dispersion of 0.02 wt% CHNC, and obtained a more sparse dispersion. The differences between the literature dispersion by Tzoumaki *et al.* (2010) and that found within this study can be seen in Figure 6B. Thereby, a more suitable dilution of the CHNC sample should be used for further chitin microscopic investigation e.g. 0.01 wt%. No microscopic images were possible of the crude SHSH due to their large size on the millimetre scale.

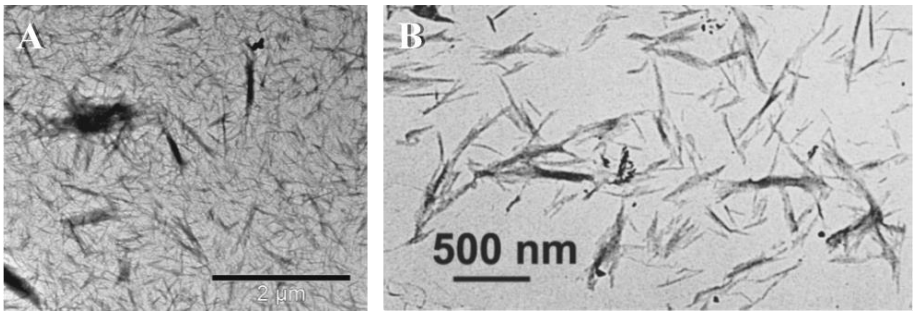

Figure 6. A:TEM micrograph (2µm) of obtained chitin nanocrystals with a 0.025 wt%, B: A TEM micrograph of 0.02 wt% CHNC taken from Tzoumaki et al. (2010).

In Figure 7, TEM micrographs of CHNC are presented, at various magnifications. Figure 7A shows a magnification with a scale bar of 2 µm, with a broad nanocrystal network, dark patches can be seen to the right of the image where the assumption is made that the layers of nanocrystals were overcrowded. Looking into another part of the grid, with a scale bar annotated of 1 µm (Figure 7B). At the greatest magnification of 500 nm (Figure 7C), it was possible to see individual CHNC organised in a network, varying in width and length.

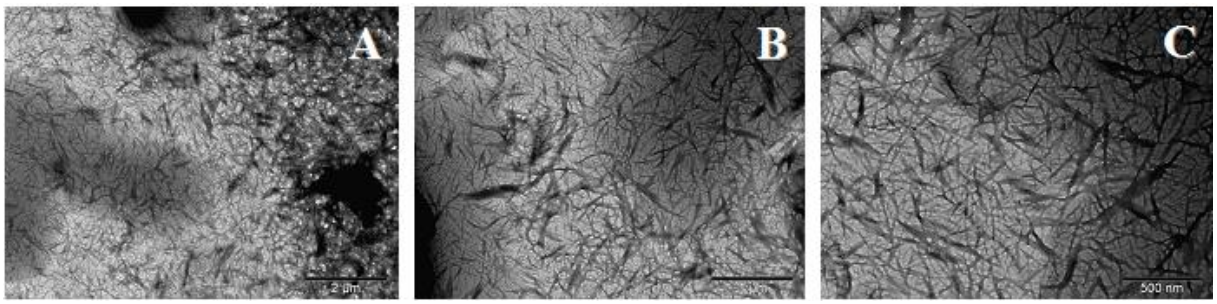

Figure 7. TEM micrographs of chitin nanocrystals (CHNC), prior to impregnation. Size of scale bar: A 2 µm; B 1 µm; C 500 nm.

3.2 IMPREGNATION OF SAMPLES

After impregnation of the support materials, drying is necessary for further analysis. The relevance of the drying step is usually neglected in the literature. However, a study was found in the literature highlighting the importance of the drying step (Toupance *et al.*, 2000). Figure 8 shows the process for impregnating the support with the copper catalyst.

Figure 8A corresponds copper nitrate trihydrate was weighed out. A dilution was made with miliQ to obtain a 5 % wt copper solution, shown in Figure 8B, details of the copper solution preparation were detailed in Equation 5. Chitin was impregnated by the means of incipient wet impregnation. It was observed that the chitin saturation point was about 3.6 mL of solution per gram chitin (see Figure 8C for completely wetted CHNC). After the addition of this amount, all copper solution was absorbed by the chitin support. Other catalyst supports were studied by Delannoy *et al*. (2006), 0.8 mL/g of different catalyst supports were used. CHNC seems to excel in solution uptake compared to conventional catalyst support.

$$M = \frac{C_{Cu}}{100} * \frac{V}{mw_{Cu}} * mw_{Cu(NO_3)_2} \qquad (5)$$

Where:

M	mass of copper nitrate trihydrate (g)
C_{Cu}	copper in the solution (%)
V	volume of MiliQ water (mL)
mw_{Cu}	molecular weight of copper (g/mol)
$mw_{Cu(NO_3)_2}$	molecular weight of copper nitrate trihydrate (g/mol)

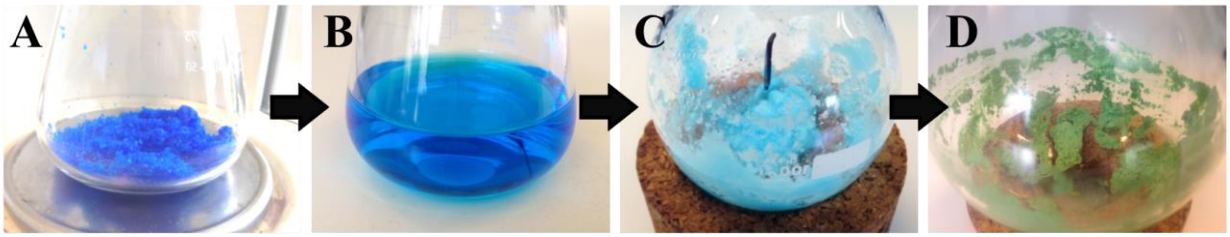

Figure 8. From left to right, A: Weighing copper; B: Addition of miliQ water to copper; C: Mixed impregnated chitin with copper; D: Drying of chitin.

A concentration of 5 % copper was used as this value has been used previously in the literature (Chang *et al.*, 2003). Figure 8C shows the impregnated CHNC after homogenisation by vigorous shaking on a rotational vortex machine. Subsequently the impregnated sample was dried in an oven, the resultant catalyst and its carrier was a dried green substance consisting of impregnated CHNC, Figure 8D.

Initially impregnated SHSH and CHNC samples were dried at 120 °C in order to perform further analysis. After heating at 120 °C for 3 h, an inhomogeneous colouration was observed for the CHNC only (Figure 9). A comparison of the XRD patterns was performed to compare the crystallinity of both regions in the sample (Figure 10). The brown coloured 5Cu-CHNC(Brown) had reduced chitin peaks (10-30°), in comparison to the green coloured sample. An increase in different formations of copper oxides (Cu^{2+}) was also found for the brown coloured sample, which were undesirable because metallic copper (Cu^{0}) was the required catalyst. Metallic copper (Cu^{0}) has been previously studies in the literature using XRD, the 2Theta values correspond well to those found in this thesis (Park *et al.*, 2007).

Figure 9. Impregnated nanocrystals (5Cu-CHNC) dried at 120 °C.

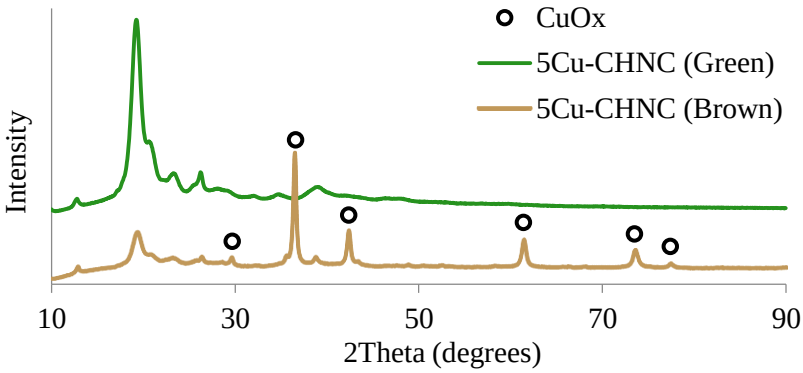

Figure 10. XRD patterns of impregnated chitin nanocrystals (5Cu-CHNC) dried at 120 °C. ○ indicates 2Theta values corresponding to undesirable copper oxides.

Crude SHSH and CHNC were then dried at a lower temperature of 60 °C. There was no effect of inhomogeneity in colour of the impregnated chitin at 60 °C observed, see Figure 11. When considering the process of drying chitin, it is also vital to consider the residence time in the oven. It was found that leaving chitin in the oven for 4 h at 60 °C gives an evenly dried sample, completely green in colour throughout (see Figure 11). A sample was dried overnight (>15 h) at 60 °C, XRD analysis (Figure 12) showed there was no indication that copper oxides were formed. Therefore if the sample is dried at 60 °C, we can assume that the drying time does not influence the production of copper oxides.

Figure 11. Impregnated chitin (5Cu-CHNC) nanocrystals dried at 60 °C.

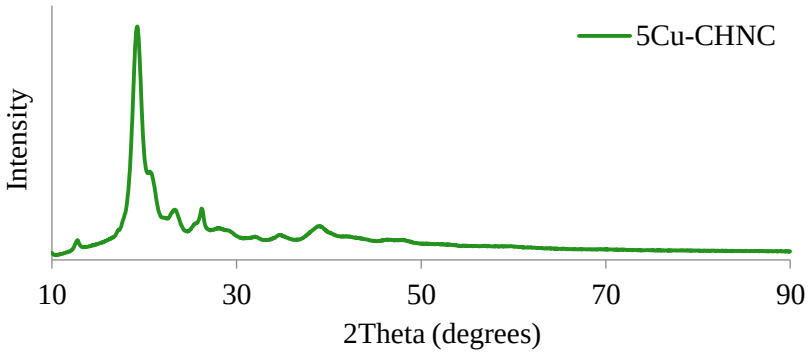

Figure 12. XRD analysis of impregnated chitin nanocrystals, dried at 60 °C.

A drying temperature of 60 °C was employed for the following experiments due to the reduced production of copper oxides in the dried, impregnated CHNC.

3.3 CALCINATION/REDUCTION OF IMPREGNATED SAMPLES

In order to produce the copper catalyst in the correct form (Cu^0), calcination/reduction was performed using various gas combinations and temperatures. Details of these conditions can be found in Table 2. Various methods were used (XRD, physisorption and microscopic investigation) to compare and contrast crude SHSH and CHNC.

3.3.1 XRD patterns of SHSH

Figure 13 shows crude SHSH, dried impregnated SHSH with 5 wt% copper solution (5Cu-SHSH) and an impregnated sample (5Cu-SHSH-N2H2(250)) reduced at 250 °C with combined nitrogen (N_2) and hydrogen (H_2) gases. Drying at 120 °C (5Cu-SHSH) resulted in a decrease in the 20° peak compared to the crude SHSH sample. Thereby indicating a less crystalline form of chitin upon impregnation and drying. Copper was reduced simultaneously with N_2 and H_2 gases to prepare sample 5Cu-SHSH-N2H2(250). After the reduction process, copper peaks can clearly be seen Figure 13 5Cu-SHSH-N2H2(250) at a 2Theta value of 43° and 50°. For copper (Cu) another peak should be visible at a 2Theta value of 74° according to Park *et al.* (2007), but up to this value was not measured due to boundary measurements.

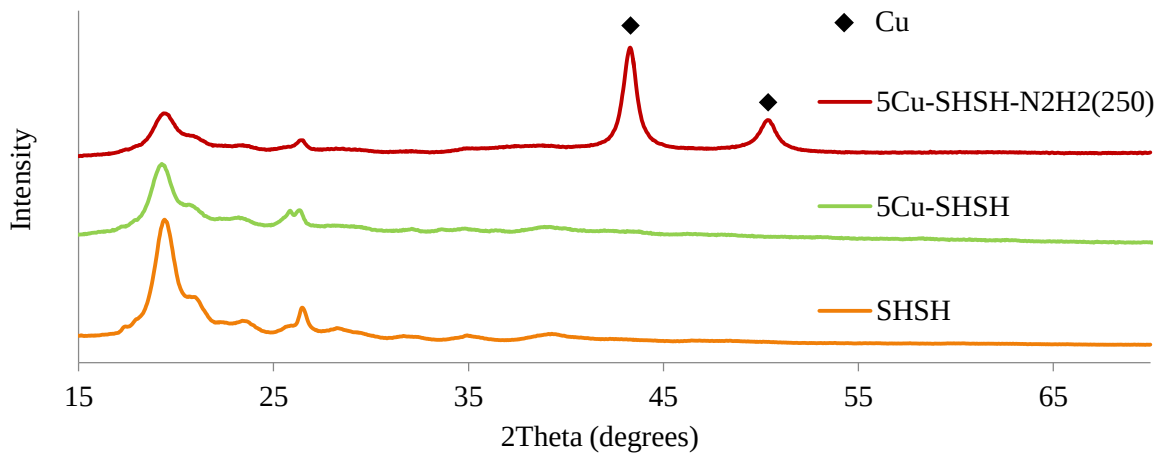

Figure 13. XRD patterns of SHSH, 5-CuSHSH and 5Cu-SHSH-N2H2(250), ◆ indicates 2Theta values corresponding to metallic copper.

Indirect reduction (2.6ii) at lower temperatures was performed to study the effects on the crystallinity of chitin and copper. A lower temperature of 200 °C was chosen for investigation as this falls below the thermal degradation temperature (T_m) of SHSH. The chitin peaks which were found between 2Theta values of 10° and 30° in Figure 14 were not visible for any of the SHSH samples prepared at lower temperature with indirect reduction (Figure 14). Although chitin is still present within the sample, this result suggests that the crystalline form of chitin is lost and must become amorphous. Formation of copper oxides occurred during N_2 treatment (5Cu-SHSH-

N2(200)) or during air followed by nitrogen treatment (5Cu-SHSH-Air(200)-N2(200)). Copper oxides are highlighted on the XRD patterns by open circles (○). When H_2 gas was subsequently passed over the same sample (5Cu-SHSH-Air(200)-N2(200)-H2(200)), metallic copper (Cu^0) was present within the sample, however that was the only crystalline material that was found using XRD.

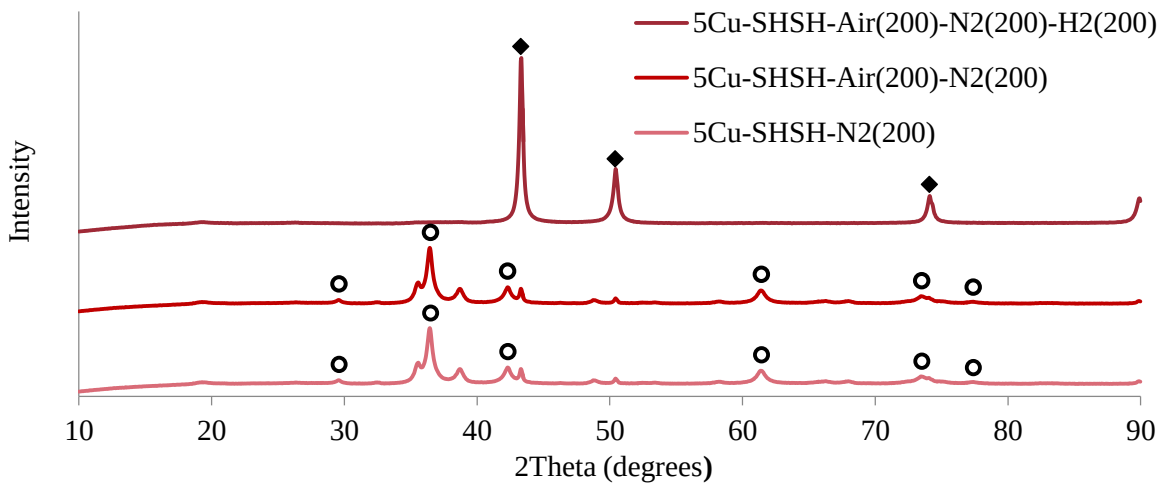

Figure 14. XRD patterns to show the effects of reduction/calcination on the crystallinity of the samples versus a dried sample without reduction/calcination. ◆ Indicates 2Theta values corresponding to copper, Copper oxide formations were indicated by ○.

3.3.2 XRD patterns of CHNC

In this section CHNC, impregnated CHNC and reduced CHNC samples were analysed using XRD to determine their crystallinity. Initially CHNC was compared to the impregnated by a 5 % copper solution (5Cu-CHNC). The 5Cu-CHNC went through a heat treatment of 60 °C to remove the water prior to analysis, whereas CHNC was dried via freeze drying. No decrease in the crystallinity of CHNC was observed. In addition to impregnation and drying no copper peaks were observed indicating the absence of copper in a crystalline form.

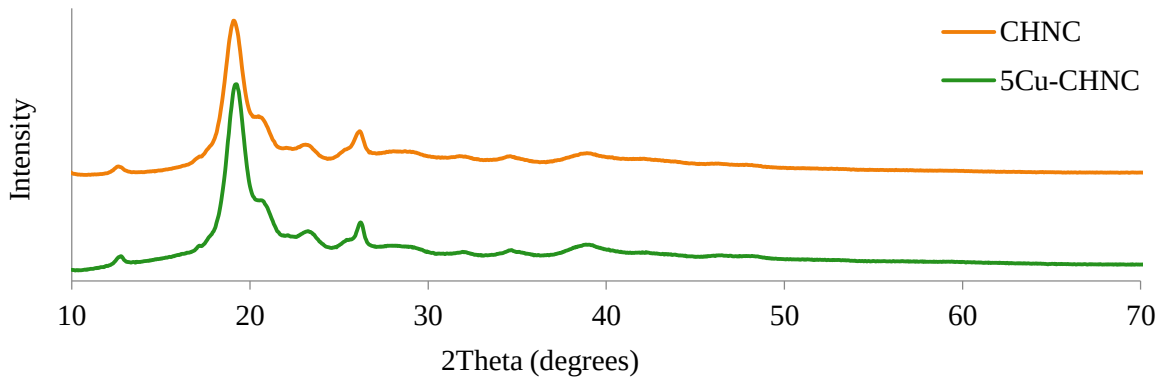

Figure 15. XRD patterns of CHNC, and impregnated 5Cu-CHNC dried at 60 °C.

After direct reduction by N_2 and H_2 gas (2.6i), metallic copper peaks (Cu) can be seen in figure 16 at 2Theta values of 43°, 50° and 74° with reduction carried out at 200 or 250 °C (5Cu-CHNC-N2H2(200) & 5Cu-CHNC-N2H2(250)). When reduction was performed at 150 °C (5Cu-CHNC-N2H2(150)), copper oxides were produced. This indicates that the reduction of copper oxides to copper occurs between in the region of 150-200 °C. Another peak should be visible at a 2Theta value of 94°, but that region was not analysed during this measurement.

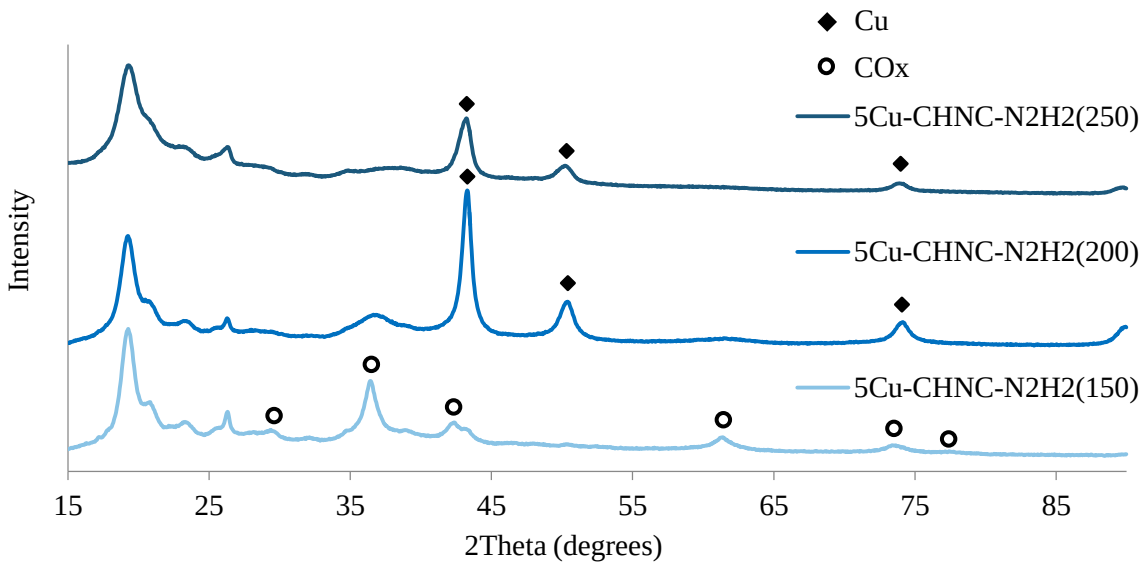

Figure 16. XRD patterns to show the effect of direct reduction temperature on the impregnated chitin nanocrystal (CHNC). Copper is indicated by ◆, Copper oxide formations were indicated by ○.

A comparison of the XRD patterns for reduced SHSH and CHNC can be seen in Figure 17. It was possible to observe crystalline chitin peaks in the region of 10-30° in both of the samples

analysed. Metallic copper peaks were also observed at the same 2Theta values found previously within the literature (Park *et al.*, 2007). In terms of metallic copper, the crystallinity in the SHSH sample was greater than that found in the CHNC sample.

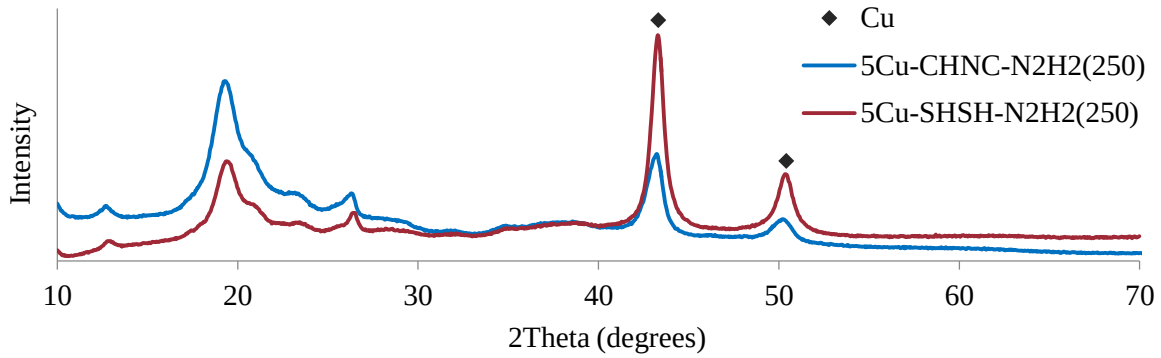

Figure 17. XRD patterns of reduced impregnated chitin from shrimp shells (5Cu-SHSH-N2H2(250)) and reduced impregnated chitin nanocrystals (5Cu-CHNH-N2H2(250)). Copper is indicated by ◆.

3.3.3 XRD patterns of 5Cu-CHNC-N2H2(brown) sample

The resultant 5Cu-CHNC(Brown) chitin sample after drying at 120 °C was reduced with N_2 and H_2 gas to determine the catalyst carrier properties compared to the 5Cu-CHNC(green) sample after reduction (Figure 18). It can be seen that the crystallinity of chitin observed in the sample was reduced upon reduction in relation to the copper peaks (5Cu-CHNC(Brown)-N2H2(250)). Copper oxides were found within the impregnated sample prior to reduction (5Cu-CHNC(Brown)). Upon reduction, strong metallic copper peaks can be seen, which directly resulted from reduction of the copper oxides (Equation 4).

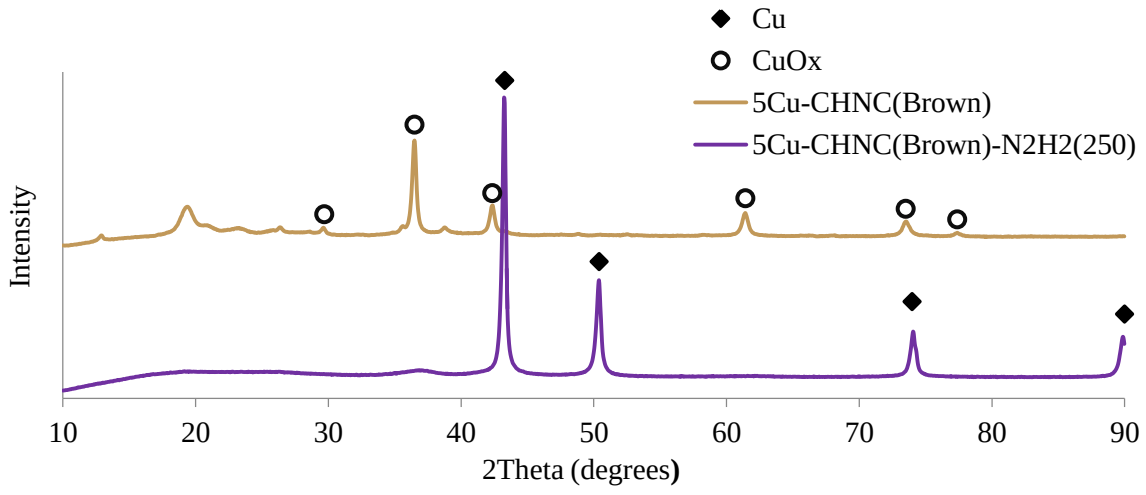

Figure 18. XRD analysis of dried impregnated chitin nanocrystals which turned brown at 120 °C (5Cu-CHNC (Brown) and reduced chitin nanocrystal 5Cu-CHNC(Brown)-N2H2(250), Copper is indicated by ◆ , Copper oxide formations were indicated by ○.

3.3.4 Physisorption

Physisorption was carried out with inert nitrogen gas to study the effects of drying and calcination/reduction conditions on the sample characteristics. Table 2 shows the different conditions for copper supported on both chitin source (SHSH & CHNC) which were tested.

3.3.4.1 SHSH

Figure 19 gives a comparison of crude SHSH versus a reduced impregnated SHSH sample (5Cu-SHSH-N2H2(250)). The physisorption graph gives us information on absorption, the amount of gas absorbed by the sample, and desorption describes the release of the gas. The reduced impregnated SHSH sample (5Cu-SHSH-N2H2(250)) was able to absorb more N_2 gas than the crude SHSH sample. This could be explained by more space for the gas to enter the catalyst support in the impregnated reduced sample in comparison to the crude SHSH. This could correspond to a structural change upon reduction. Both samples experienced an episode during desorption, a barrier was present which occurred at a relative pressure of 0.5. More information on the pore size and surface area (BET) of the materials can be found below in Table 4.

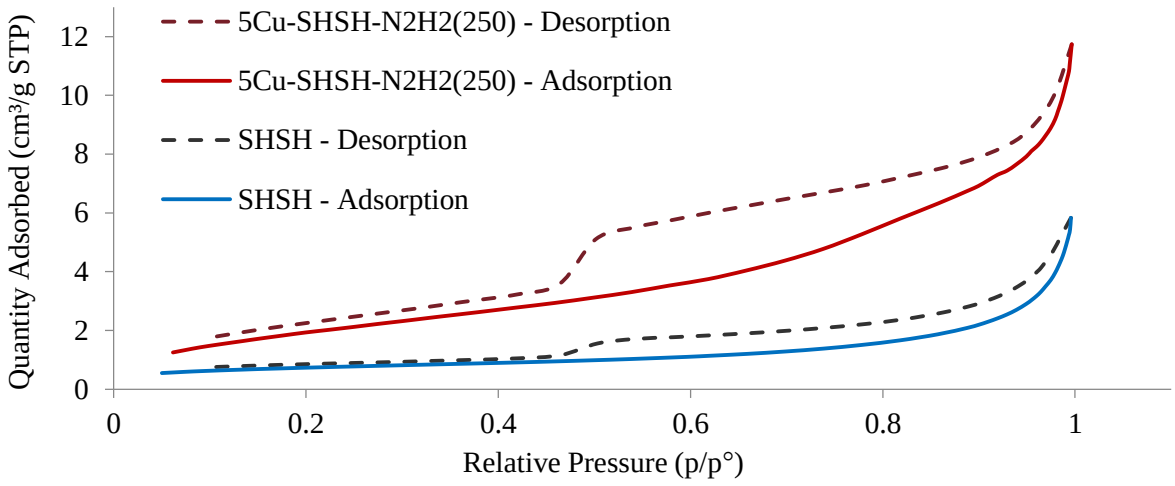

Figure 19. Physisorption graph comparison of crude chitin from shrimp shells (SHSH) and reduced, impregnated SHSH.

3.3.4.2 CHNC

Physisorption data was collected for CHNC after preparation and the effect of temperature (150, 200, & 250 °C) during direct reduction was also studied. The results can be found in Figure 20. When comparing CHNC to SHSH, without impregnation or reduction, it can be seen that both materials absorb the same volume of gas. However, upon desorption, SHSH showed a barrier had to be overcome, whereas CHNC did not. When studying the effect of thermal treatment during reduction (150, 200 and 250 °C) of CHNC, a stepwise increase in the amount of N_2 gas absorbed was found with increasing temperature. The increase was found to be stepwise with the greatest volume of gas absorbed by the temperature reduced at 250 °C (5Cu-CHNC-N2H2(250)). At a relative pressure value of 1, this stepwise increase in the volume absorbed with increasing reduction temperature was not observed. This could be due to a discrepancy in the measurement of the sample prepared with reduction at 250 °C. This should be investigated further. The desorption was also affected by the reduction temperature (Figure 20). A desorption barrier was found upon reduction at a relative pressure of 0.5 and the intensity of the barrier increased with increased temperature.

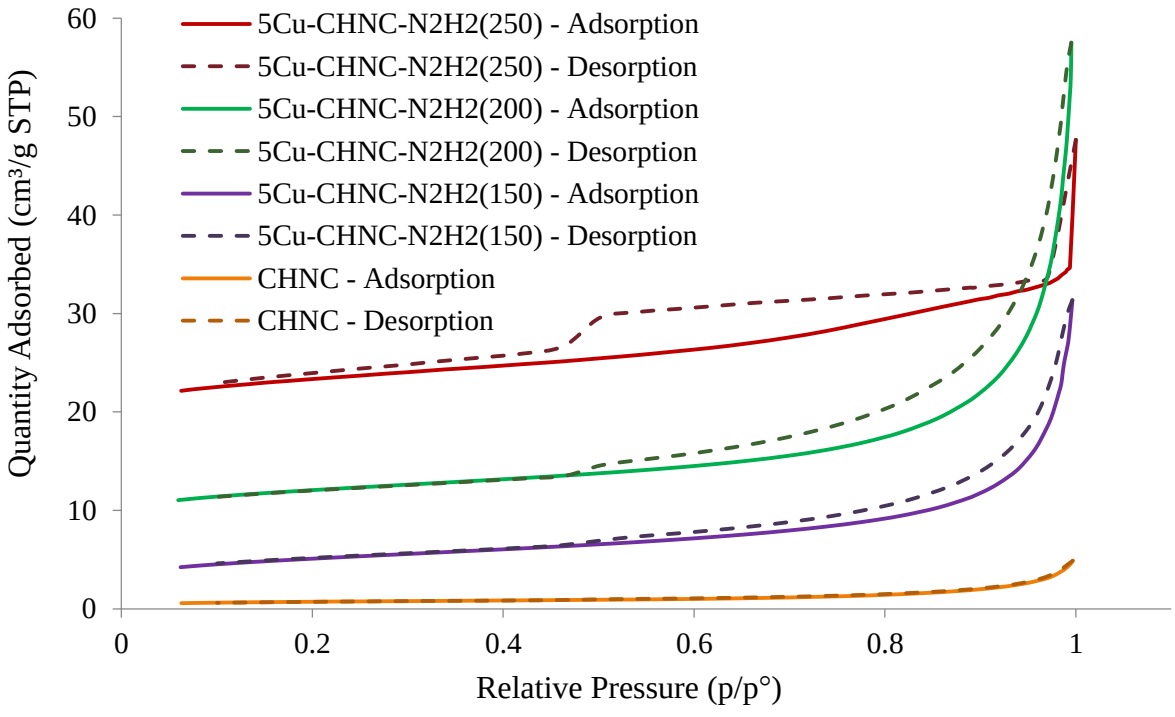

Figure 20. Physisorption graph of chitin nanocrystals (CHNC), with different reduction temperatures in the range of 150 to 250 °C

A comparison was made to determine which material, CHNC or SHSH, could absorb more gas at the same reduction temperature. After impregnation and reduction at 250 °C, CHNC could absorb a greater volume of gas due to structural changes upon heating in comparison to the counterpart SHSH sample.

3.3.4.3 Comparison of the resulting pore sizes in the catalyst carriers

In terms of catalysis for any reaction, the greater the surface area of the catalyst, the more surface is available for the reactants. It is also necessary to study the particle size of the catalyst support material. In this study the surface area and average pore diameter were measured for SHSH and CHNC, and also the influence of the reduction temperature was also studied (Table 4). The calculated BET surface area indicates the area of catalyst carrier, not strictly the amount of exposed copper available for catalysis. For SHSH, the BET surface area increased upon reduction at a temperature of 250 °C. The average pore diameter of SHSH also decreased by 25 % upon reduction at 250 °C. Ideally, the copper particle size should be smaller than the average pore diameter of the catalyst support. This will be discussed further in section 3.3.5.

Prior to reduction, CHNC had a comparable BET surface area value to the SHSH sample. The average pore diameter was also similar. Upon reduction of CHNC at 150 °C, the BET surface area increased and the average pore diameter reduced. With a reduction temperature of 200 °C, the surface area increased, as well as the average pore diameter. Upon reduction at 250 °C, the BET surface area and the pore diameter values both reduced. This could have been caused by a discrepancy in the measurement which was discussed in the previous section (3.3.4.2). It could also be explained through the thermal degradation temperature of CHNC; reduction was performed at a temperature above the T_m of 215 °C.

Table 4. Sample names and reduction temperatures, BET surface area, average pore width

Sample	**Reduction temperature (°C)**	**BET Surface Area (m^2/g)**	**Average pore diameter (nm)**
SHSH	-	2.65	12.10
5Cu-SHSH-N2H2	250	7.63	9.03
CHNC	-	2.46	11.57
5Cu-CHNC-N2H2	250	13.40	5.90
5Cu-CHNC-N2H2	200	14.54	8.49
5Cu-CHNC-N2H2	150	11.41	7.17

3.3.5 Microscopic investigation

Microscopy gave an insight into the size and how the nanocrystals were orientated, as well as the size of the copper particles on the supporting material. SEM was used to give a visual representation of CHNC after direction reduction (5Cu-CHNC-N2H2(200)). Using this technique, it was not possible to see copper particles on the surface of the CHNC. In Figure 21A, a particle was observed. It was not possible to distinguish individual nanocrystals, which could be due to the magnification of the microscope. In Figure 21B, it is possible to see stacked layers and order at a higher level of magnification (1µm) compared to Figure 21A (40µm). On Figure 21B, an EDX analysis was performed to give information on the elements which were present in the visualised area of the sample (Figure 21C). From this analysis, it was possible to locate copper at a concentration of 5.1 wt% in the visualised area of the sample. Also present was a large concentration of carbon and oxygen, which corresponds to the chitin support material (see Figure 1). Per chitin molecule found within the CHNC image analysed (containing 5 oxygen molecules), there is roughly 1 copper particle present, based on weight (wt).

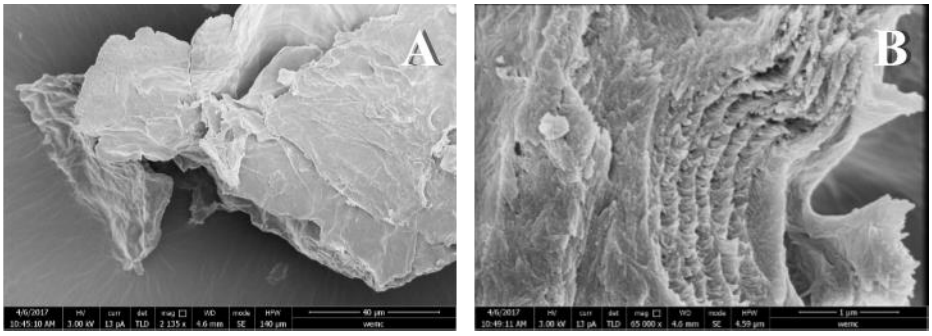

C	
Element	**Wt%**
C	71.8
O	22.8
Cu	5.1

Figure 21. A: SEM image of 5Cu-CHNC-N2H2(200), B: magnification of SEM image A SEM image. C:EDX spectrum of 5Cu-CHNC-N2H2(200),

One observation was that samples stored in methanol for a prolonged time began to discolour, indicating that leaching of copper took place. Therefore fresh samples were used for all image analysis.

3.3.5.1 Sizing of copper particles

The size of the copper particles could be measured using TEM micrographs. Particle size measurement was done by a program called Fiji is Just, ImageJ. TEM images show dark irregular and spherical shapes (Figure 22A). Particles were assumed to be overlapping each other, therefore it was difficult to measure each individual particle. The contrast and brightness of the surface area was altered for clear boundary definition for each particle, see Figure 22B.

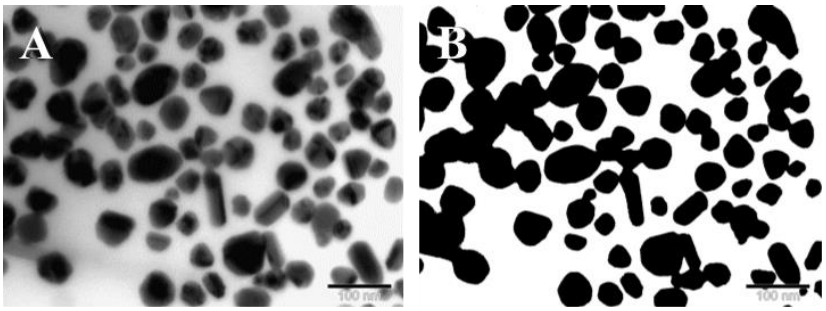

Figure 22. A: TEM micrograph of impregnated chitin nanocrystals (5Cu-CHNC-N2H2(200), B simplified image of micrograph A

The copper particle diameter (d_{Cu} in nanometres) was calculated by assuming spherical particle shapes by means of the following equation.

$$d_{Cu} = 2\sqrt{\frac{a}{\pi}} \qquad (6)$$

Where:

d_{Cu}	diameter (nm)
a	area (dependent of the size of TEM scale bar)

A sample of SHSH was also impregnated and reduced at a temperature of 250 °C (5Cu-SHSH-N2H2(250)), the resulting sample was imaged using TEM, see Figure 23. An even dispersion of copper was found throughout the impregnated and reduced sample. The carrier material (SHSH) which supported the copper particles was randomly ordered. ImageJ software was used to individually select every particle and a frequency count is made. These results can be seen in

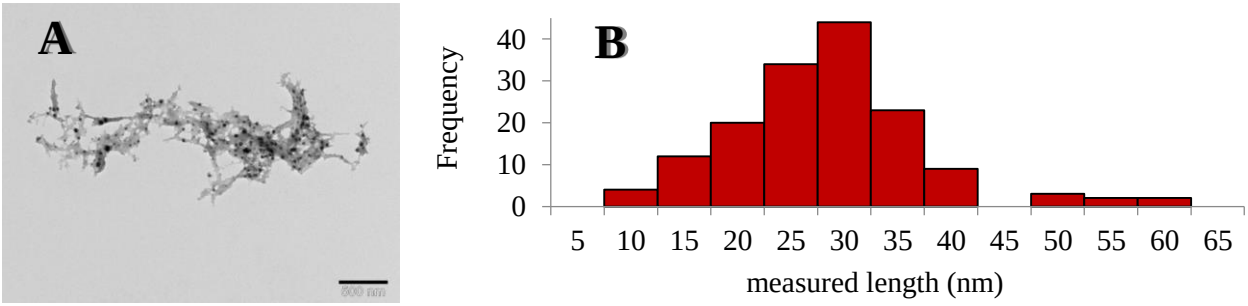

Figure 23. A: TEM image of 5Cu-SHSH-N2H2(250) at 500 nm. B: Histogram of sample count of copper particles for the sample 5Cu-SHSH-N2H2(250).

histogram (Figure 23B).

The copper particle size distribution on SHSH indicates copper particles ranging from 5 to 65 nm, with an average of 30 nm.

The CHNC catalyst support was also studied with TEM to determine the size of the copper particles. The sample was impregnated and reduced at a temperature of 200 °C (5Cu-CHNC-N2H2(200)) (see Figure 24). Please note that the temperature of reduction for CHNC was lower than that used for SHSH (200 vs. 250 °C). A broad dispersion of copper particles were visible throughout the sample looking into different grids. In Figure 24, two distinct areas were observed, each with a different particle size distribution of copper. A large cluster of smaller copper particles are visible (Figure 24A) as well as a small cluster underneath it with larger particles (Figure 24B).

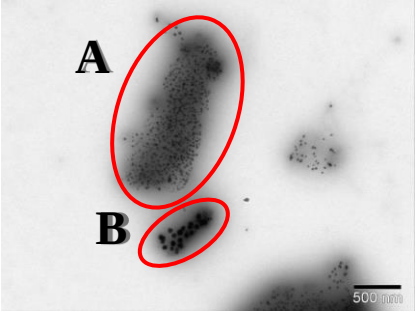

Figure 24. TEM micrograph of sample 5Cu-CHNC-N2H2(200)

Copper particles were measured in the large cluster of smaller particles (Figure 24A). A close-up TEM micrograph of the copper particles was used for the size measurement (Figure 25A). Within this region, an average copper particle size of 15 was observed (Figure 25B).

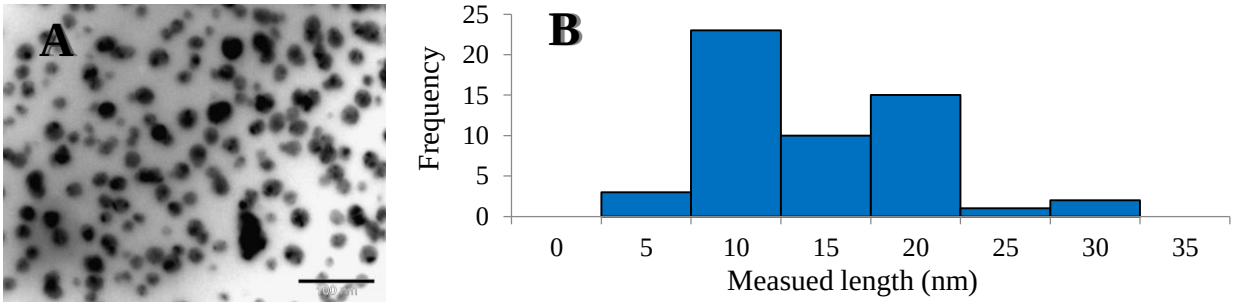

Figure 25. A: TEM image of 5Cu-CHNC-N2H2(200) at 100 nm. B: Histogram of sample count of copper particles for the sample 5Cu-CHNC-N2H2(200).

Within the smaller region of larger particle (Figure 24B), another copper particle size count was performed using a close-up micrograph (Figure 26A). Within this area of the sample an average copper particle size of 20 nm was measured (Figure 26B).

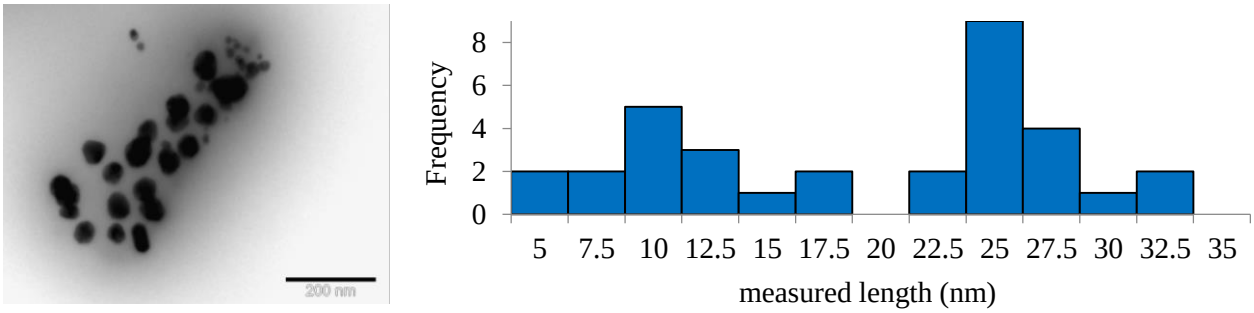

Figure 26. A: TEM image of 5Cu-CHNC-N2H2(200) at 200 nm. B: Histogram of sample count of copper particles in the sample 5Cu-CHNC-N2H2(200).

An average particle size of the large and small copper particle distributions for 5CU-CHNC-N2H2(200) was calculated to be 20 nm. The results for sizing of the copper particles give an indication of the average size, the micrographs presented here only take into consideration a very small 2D image of the sample. However further analysis is necessary to give a true representation of the size. According to the data presented, the copper particles are on average larger than the average pore size diameters of both catalyst supports (SHSH and CHNC). It can be assumed that some copper particles are small enough to enter the pores of the catalyst support material. From the TEM micrographs, especially on the SHSH support (Figure 25A(SHSH micrograph)), it could be assumed that copper particles are on the surface of the support material, rather than within its pores. Further examination is needed to study how the catalyst carrier performs and if copper is recoverable.

3.4 CATALYSING THE HYDROGENATION OF GLUCOSE AND FRUCTOSE TO SORBITOL – SUCCESS OF THE CATALYST CARRIERS

In order to examine the success of the catalyst support material, a catalysed reaction needs to be carried out with CHNC and SHSH materials. In this study, the hydrogenation of glucose to form sorbitol was performed in the laboratory at 25 °C as an initial assessment of 5Cu-SHSH-N2H2(250). High performance liquid chromatography (HPLC) was used to analyse the amount of fructose and sorbitol formed during the reaction. A sample of the reaction liquid was taken every 15 min for 4 h. HPLC data showed no decrease in glucose, nor production of fructose or sorbitol peaks in any of the samples. Reasons why the reaction did not proceed could be linked to the experimental set-up, including an incorrect temperature of the vessel, the concentration of catalyst or reaction time. Also, the analytical method for measuring the levels of glucose, fructose and sorbitol could also affect the data produced. Prior to analysis, there were issues with the HPLC column, which may have influenced the results of the reaction. Please see section 5 for more details of recommendations for future work.

4 CONCLUSIONS

The aim of this study was to investigate the potential of chitin nanocrystals (CHNC) and shrimp shells (SHSH) as a catalyst support for metallic copper. A method was developed in this study to impregnate, to dry and to calcinate/reduce the support material containing the copper catalyst. Differences between CHNC and SHSH have been investigated and a comparison of their physiochemical characteristics has been performed using techniques such as FTIR, XRD and TGA.

Conditions for the impregnation, drying and calcination/reduction of the catalyst carrier materials were studied and the most favourable were further investigated. It was possible to disperse small copper particles ranging in length between 15-30 nm with chitin (both SHSH and CHNC) as a catalyst support material by means of incipient wetness impregnation. Initially drying of the impregnated sample was carried out at 120 °C, however this resulted in the production of undesirable copper oxides. Drying the impregnated sample at 60 °C showed no copper oxide formations. To obtain metallic copper, it was necessary to perform the calcination/reduction at a temperature of 200 °C. Direct or indirect reduction and calcination were studied for SHSH, and it was concluded that direct reduction (N_2/H_2) was more favourable due to chitin crystallinity and the production of metallic copper.

Once the method for production of the catalyst carried was developed, it was possible to determine which carrier material was more suitable, SHSH or CHNC. Based on thermal analysis, SHSH seems more favourable due to a higher decomposition temperature. By studying the crystallinity of the catalyst support materials, CHNC was more favourable due to the presence of crystalline chitin and metallic copper. The size of the copper particles on both of the catalyst support materials was comparable, both materials contained small evenly dispersed copper particles. Based on the physisorption analysis, the catalyst support materials have comparable surface areas and average pore diameters. However after impregnation and direct reduction, including thermal treatment, CHNC was more favourable due to a larger surface area and a smaller average pore diameter.

Considering all of the analysis performed within this study, it is concluded that CHNC is a suitable catalyst support material. The most promising conditions for catalyst support production involved direct reduction using N_2 and H_2 gas at a temperature of 200 °C (5Cu-CHNC-N2H2(200)). Further work is necessary to study the benefits of using a CHNC support material, and to confirm the findings presented here.

5 FUTURE WORK

Future studies are recommended to further explore and to completely understand how the catalyst support materials behave during the catalysed reaction. Many methods of catalyst carrier production and analysis have been performed, however further clarification is necessary. During this study, it was not possible to explore all interesting paths, due to time restrictions and equipment failure. In this section, some ideas for continuation of the project are given.

5.1 CATALYST SUPPORT PREPARATION

The chitin from shrimp shells obtained from Sigma-Aldrich does not indicate the amount of acetyl groups present or any residual proteins which could influence the pore size and interactivity with the copper. With the knowledge obtained in this thesis, it is possible to eliminate some steps from the procedure described in 3.1. The protonation step (addition of KOH) could be discarded from the nanocrystal preparation as it is believed to have already been carried out by the manufacturer.

Within this thesis, a solution of 5 wt% copper solution was used to impregnate the support material, as this was considered to be suitable based on the literature. Different loading percentages could be studied further as increasing the load of catalyst could improve the catalysis yield and reaction time.

Another interesting aspect would be the effect of impregnation at different pH values. The isoelectric point of a substance determines its orientation within aqueous conditions. In this work, the chitin nanocrystals were freeze dried after preparation at a pH value of 3. In future work, the effects of pH at the stage of freeze drying on the resulting CHNC sample should be studied further. This could influence the average pore diameter of the support material, as well as the pH of the catalyst solution chosen for impregnation of the carrier.

Comparable techniques as incipient wet impregnation, e.g. adsorption, wet impregnation, homogeneous deposition precipitation can be done to investigate a faster/cheaper/higher yielding way to impregnate a sample.

5.2 ANALYTICAL TECHNIQUES TO BE CONSIDERED

In order to measure the length and width of the CHNC, further dilution of the sample was necessary to produce a clear TEM image. In this thesis, a CHNC concentration of 0.025 wt% was initially used and resulted in a dense nanocrystal dispersion. As a starting point for future work, a concentration of 0.01 wt% is suggested.

One technique that was not available during this project was chemisorption because the required gas combination was not available. With this technique, it is possible to measure the strength of the interaction between the copper catalyst and the support material. This technique can also be used to measure the (copper) catalyst characteristics e.g. leaching capabilities of the catalyst.

X ray analysis , curve deconvolution of data, diffraction data smoothed by Savitsky-Golay filter with the use of a second-order polynomial regression and fit with Gaussian-Lorentzian like shape peak fit (Goodrich & Winter, 2007). With this data analysis, it is possible to determine the Miller indices (hkl values), which provides data on the internal planes within a crystal lattice.

5.3 PERFORMING CATALYSED REACTION

In order to assess how the catalyst support material actually performs, it is necessary to carry out the catalysed reaction. Due to the large volume of chitin which is readily available for valorisation from shrimp shell waste, a number of different catalysts could be supported. Future work with copper reactions should be carried out and compared to other catalysts and support materials to determine the most beneficial conversion yields. Other catalysts could also be explored using a chitin based support material.

ACKNOWLEDGEMENTS

I would like to thank my supervisor Costas Nikiforidis for giving me the opportunity to do my thesis under his wing and giving me the freedom of thought and supervision needed to succeed in this endeavour.

Tomas, you stirred the ship and gave me some direction and insight into possible ideas to research. Thank you for putting up with me with all the annoying questions I had to bug you with.

Thank you Gerben for taking your time to obtain beautiful TEM and SEM images.

Also I would like to give my kindest regards to Anja Jansen for giving me all the support and self-confidence throughout my Masters study.

Thank you dear colleagues in the open office for being serious, but also for sharing some fun once in a while. Special thanks to Walter and Tijmen which made my Masters thesis more enjoyable.

Mom and Dad you have supported me throughout, thank you for your support.

Last but not least, my girlfriend Katherine whom I would like to refer to “the root to my tree”, the person that gave me motivation and insight during my thesis.

REFERENCES

Chang, F. W., Kuo, W. Y., & Lee, K. C. (2003). Dehydrogenation of ethanol over copper catalysts on rice husk ash prepared by incipient wetness impregnation. *Applied Catalysis A: General*, *246*(2), 253-264.

Delannoy, L., El Hassan, N., Musi, A., Le To, N. N., Krafft, J. M., & Louis, C. (2006). Preparation of supported gold nanoparticles by a modified incipient wetness impregnation method. *The Journal of Physical Chemistry B*, *110*(45), 22471-22478.

Goodrich, J. D., & Winter, W. T. (2007). α-Chitin nanocrystals prepared from shrimp shells and their specific surface area measurement. *Biomacromolecules*, *8*(1), 252-257.

Gopalan Nair, K., & Dufresne, A. (2003). Crab shell chitin whisker reinforced natural rubber nanocomposites. 1. Processing and swelling behavior. *Biomacromolecules*, *4*(3), 657-665.

Jang, M. K., Kong, B. G., Jeong, Y. I., Lee, C. H., & Nah, J. W. (2004). Physicochemical characterization of α-chitin, β-chitin, and γ-chitin separated from natural resources. *Journal of Polymer Science Part A: Polymer Chemistry*, *42*(14), 3423-3432.

Khor, E., & Lim, L. Y. (2003). Implantable applications of chitin and chitosan. *Biomaterials*, *24*(13), 2339-2349.

Köll, P., Borchers, G., & Metzger, J. O. (1991). Thermal degradation of chitin and cellulose. *Journal of Analytical and Applied Pyrolysis*, *19*, 119-129.

Lin, N., Huang, J., & Dufresne, A. (2012). Preparation, properties and applications of polysaccharide nanocrystals in advanced functional nanomaterials: a review. *Nanoscale*, *4*(11), 3274-3294.

Liu, P., Sehaqui, H., Tingaut, P., Wichser, A., Oksman, K., & Mathew, A. P. (2014a). Cellulose and chitin nanomaterials for capturing silver ions (Ag+) from water via surface adsorption. *Cellulose*, *21*(1), 449-461.

Liu, X., Wang, X., Yao, S., Jiang, Y., Guan, J., & Mu, X. (2014b). Recent advances in the production of polyols from lignocellulosic biomass and biomass-derived compounds. *RSC Advances*, *4*(90), 49501-49520.

Matsuoka, A., Isogawa, T., Morioka, Y., Knappett, B. R., Wheatley, A. E., Saito, S., & Naka, H. (2015). Hydration of nitriles to amides by a chitin-supported ruthenium catalyst. *RSC Advances*, *5*(16), 12152-12160.

Munnik, P., Wolters, M., Gabrielsson, A., Pollington, S. D., Headdock, G., Bitter, J. H.,... & De Jong, K. P. (2011). Copper nitrate redispersion to arrive at highly active silica-supported copper catalysts. *The Journal of Physical Chemistry C*, *115*(30), 14698-14706.

Park, B. K., Jeong, S., Kim, D., Moon, J., Lim, S., & Kim, J. S. (2007). Synthesis and size control of monodisperse copper nanoparticles by polyol method. *Journal of colloid and interface science*, *311*(2), 417-424.

Perrin, E., Bizot, H., Cathala, B., & Capron, I. (2014). Chitin nanocrystals for Pickering high internal phase emulsions. *Biomacromolecules*, *15*(10), 3766-3771.

Pinto, P. X., Al-Abed, S. R., & Reisman, D. J. (2011). Biosorption of heavy metals from mining influenced water onto chitin products. *Chemical Engineering Journal*, *166*(3), 1002-1009.

Poletto, M., Ornaghi, H. L., & Zattera, A. J. (2014). Native cellulose: structure, characterization and thermal properties. *Materials*, *7*(9), 6105-6119.

Sikorski, P., Hori, R., & Wada, M. (2009). Revisit of α-chitin crystal structure using high resolution X-ray diffraction data. *Biomacromolecules*, *10*(5), 1100-1105.

Synowiecki, J., & Al-Khateeb, N. A. (2003). Production, properties, and some new applications of chitin and its derivatives. *Critical Reviews in Food Science and Nutrition*, *43(2)*, 145-171.

Toupance, T., Kermarec, M., & Louis, C. (2000). Metal particle size in silica-supported copper catalysts. Influence of the conditions of preparation and of thermal pretreatments. *The Journal of Physical Chemistry B*, *104*(5), 965-972.

Tzoumaki, M. V., Moschakis, T., & Biliaderis, C. G. (2009). Metastability of nematic gels made of aqueous chitin nanocrystal dispersions. *Biomacromolecules*, *11*(1), 175-181.

Tzoumaki, M. V., Karefyllakis, D., Moschakis, T., Biliaderis, C. G., & Scholten, E. (2015). Aqueous foams stabilized by chitin nanocrystals. *Soft matter*, *11*(31), 6245-6253.

Wada, M., & Saito, Y. (2001). Lateral thermal expansion of chitin crystals. *Journal of Polymer Science Part B: Polymer Physics*, *39*(1), 168-174.

Wang, Y., Li, Y., Liu, S., & Li, B. (2015). Fabrication of chitin microspheres and their multipurpose application as catalyst support and adsorbent. *Carbohydrate polymers*, *120*, 53-59.

Wanjun, T., Cunxin, W., & Donghua, C. (2005). Kinetic studies on the pyrolysis of chitin and chitosan. *Polymer Degradation and Stability*, *87*(3), 389-394.

Wu, J., & Meredith, J. C. (2014). Assembly of chitin nanofibers into porous biomimetic structures via freeze drying. *ACS Macro Letters*, *3*(2), 185-190.

Yan, N., & Chen, X. (2015). Don't waste seafood waste: Turning cast-off shells into nitrogen-rich chemicals would benefit economies and the environment. *Nature*, *524*(7564), 155-158.

Yu, Z., Xu, Z., & Lau, D. (2014). Effect of acidity on chitin–protein interface: a molecular dynamics study. *BioNanoScience*, *4*(3), 207-215.

Zeng, J. B., He, Y. S., Li, S. L., & Wang, Y. Z. (2011). Chitin whiskers: An overview. *Biomacromolecules*, *13*(1), 1-11.

Zhang, Y., Jiang, J., Liu, L., Zheng, K., Yu, S., & Fan, Y. (2015). Preparation, assessment, and comparison of α-chitin nano-fiber films with different surface charges. *Nanoscale research letters*, *10*(1), 226.